JACS
JOURNAL OF THE AMERICAN CHEMICAL SOCIETY

ARTICLE

pubs.acs.org/JACS

Synergetic Effect of Surface and Subsurface Ni Species at Pt−Ni Bimetallic Catalysts for CO Oxidation

Rentao Mu,[†] Qiang Fu,*[,†] Hong Xu,[†] Hui Zhang,[†] Yuying Huang,[‡] Zheng Jiang,[‡] Shuo Zhang,[‡] Dali Tan,[†] and Xinhe Bao*[,†]

[†]State Key Laboratory of Catalysis, Dalian Institute of Chemical Physics, Chinese Academy of Sciences, Dalian 116023, P.R. China

[‡]Shanghai Synchrotron Radiation Facility, Shanghai Institute of Applied Physics, Chinese Academy of Sciences, Shanghai 201204, P.R. China

Supporting Information

ABSTRACT: Various well-defined Ni−Pt(111) model catalysts are constructed at atomic-level precision under ultra-high-vacuum conditions and characterized by X-ray photoelectron spectroscopy and scanning tunneling microscopy. Subsequent studies of CO oxidation over the surfaces show that a sandwich surface (NiO_{1-x}/Pt/Ni/Pt(111)) consisting of both surface Ni oxide nanoislands and subsurface Ni atoms at a Pt(111) surface presents the highest reactivity. A similar sandwich structure has been obtained in supported Pt−Ni nanoparticles via activation in H_2 at an intermediate temperature and established by techniques including acid leaching, inductively coupled plasma, and X-ray adsorption near-edge structure. Among the supported Pt−Ni catalysts studied, the sandwich bimetallic catalysts demonstrate the highest activity to CO oxidation, where 100% CO conversion occurs near room temperature. Both surface science studies of model catalysts and catalytic reaction experiments on supported catalysts illustrate the synergetic effect of the surface and subsurface Ni species on the CO oxidation, in which the surface Ni oxide nanoislands activate O_2, producing atomic O species, while the subsurface Ni atoms further enhance the elementary reaction of CO oxidation with O.

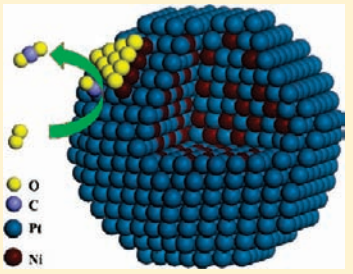

INTRODUCTION

Bimetallic catalysts are widely used in many heterogeneous catalytic processes. With rational design of the catalyst structure, enhanced stability, activity, and selectivity can be achieved in comparison to their parent metals.[1−11] For example, modifying Pt nanoparticles (NPs) with Au clusters can stabilize Pt oxygen-reduction fuel-cell electrocatalysts against dissolution under potential cycling regimes.[7] The oxygen reduction reaction (ORR) activity has been increased by 1 order of magnitude on the $Pt_3Ni(111)$ surface compared to the corresponding Pt(111) surface.[9] Improved selectivity of oxidation of alcohols to aldehydes with O_2 was obtained by alloying Pd nanocrystals with Au.[6]

Among the bimetallic catalytic systems, the most frequently studied are Pt-based bimetallic catalysts, which are often used in many important reactions, such as ORR,[8,9,12−23] hydrogenation,[10,24−31] water−gas shift (WGS),[32] and oxidation reactions.[33−50] In past decades, extensive research efforts have been made to prepare highly efficient catalysts and illustrate the reaction mechanism in the Pt-based bimetallic systems. It has been well established that Pt-skin structures with transition metals (TMs) in the subsurface regions are the active surface phase in ORR, hydrogenation, and WGS. The d-band center of the Pt-skin surfaces often shifts away from the Fermi level. Adsorption of both atomic and molecular adsorbates such as H, O, OH, O_2, and CO on the surfaces is weakened, which consequently increases the catalytic activity of these reactions. Both the compressive strain effect and the ligand effect contribute to the modification of the surface catalytic properties.[12,32,51,52] Moreover, the Pt-skin surfaces are indeed the stable surface structure in acid solutions for the ORR reactions[9,14,17−19,53] and in the reductive atmospheres for the hydrogenation reactions.[54−56]

In contrast, there is no consistent picture for the active surface structure of the Pt-based bimetallic catalysts in oxidation reactions, such as the CO oxidation. Over Pt−Fe catalysts, a "bifunctional mechanism" was proposed, in which both Pt and Fe need to be present at the topmost surface, acting as adsorption sites for CO and O_2, respectively.[35,38,40,57,58] However, core−shell NPs made of a TM core (Ru, Rh, Ir, or Pd) covered with a Pt shell demonstrate better activity and selectivity of preferential CO oxidation (PROX) in H_2-rich environments than the corresponding monometallic and bulk nonsegregated bimetallic nanoalloys.[43−45] In addition, isolated monometallic NPs have been proposed as the active structure in Pt−Ni[41] and Pt−Co[42] catalysts for CO PROX.

On the basis of a joint research effort from model systems and real catalysts, we have identified monolayer-dispersed FeO nanostructure on Pt surfaces to be the active Pt−Fe surface for the CO oxidation. The key aspect is that coordinatively unsaturated

Received: October 27, 2010
Published: January 19, 2011

dx.doi.org/10.1021/ja109483a | J. Am. Chem. Soc. 2011, 133, 1978–1986

ferrous (CUF) atoms confined at edges of the two-dimensional (2D) FeO nanoislands help to activate O_2 and produce highly reactive O atoms.[46] In the present article, we will show that the same interface confinement effect can be applied to Pt−Ni catalytic systems. Monolayer NiO nanostructures have been stabilized on Pt surfaces, which are highly active for the CO oxidation. Moreover, the promotional effect of subsurface Ni atoms on the reaction has been revealed. A sandwich Pt−Ni structure containing both surface Ni oxide and subsurface Ni presents improved reactivity. Since the sandwich surface structure can be simply obtained by activation of the Pt−TM catalysts in H_2, which is often applied as pretreatment of powdered catalysts, this highly active structure should be widely present in many bimetallic catalyst systems, in which the synergetic catalytic mechanism is indeed dominant. On the other hand, our results indicate that the methodology applied here, in which studies on model catalysts are correlated with those from supported catalysts, is of general interest to understanding the bimetallic catalytic mechanism in one aspect and to fabrication of highly efficient bimetallic catalysts in another aspect.

EXPERIMENTAL SECTION

Ni−Pt(111) Model Systems. Experiments on the model catalysts were carried out in an Omicron multiprobe ultra-high-vacuum (UHV) system, which consists of a preparation chamber, a spectroscopic chamber, and a microscopic chamber.[59−61] The system is equipped with a hemispherical energy analyzer (Omicron EA125 5-channeltron) for X-ray photoelectron spectroscopy (XPS) and ultraviolet photoelectron spectroscopy (UPS), a variable-temperature scanning tunneling microscope (Omicron VT STM/AFM), a high-resolution electron energy loss spectroscope (HREELS; LK ELS5000), a photoemission electron microscope (Focus IS-PEEM), and an independent chamber for sample preparation. A clean Pt(111) surface was obtained through cycled Ar^+ sputtering (1.5 kV, 7.5×10^{-6} mbar) and UHV annealing at 1060 K until no contamination was detected by XPS and STM. The Ni evaporation source was made up of a tungsten filament (99.95% purity, Johnson Matthey) wrapped with Ni wire (ϕ = 0.1 mm, Alfa Aesar, 99.994%). Deposition of Ni was carried out by passing constant current through the tungsten filament. Coverage of Ni overlayers was controlled by the evaporation time, with the deposition rate of 0.011 monolayer (ML)/min. Gases, such as O_2 (99.9999%) and CO (99.999%), were introduced into the vacuum by backfilling the chambers. Gas exposure is given in units of langmuir (1 L = 1×10^{-6} Torr·s). XPS spectra were acquired using Mg Kα (1253.6 eV) radiation with the pass energy of 30 eV. UPS signals were recorded in the normal emission direction using He II (40.8 eV) as the excitation source. STM images were acquired in constant current mode using a W-tip at room temperature.

Supported Pt−Ni Nanoparticles. Pt−Ni NPs supported on carbon black (CB) were prepared by wetness co-impregnation using H_2PtCl_6 and $Ni(NO_3)_2$ as the precursors. After aging and drying overnight at 60 °C, fresh Pt−Ni/CB catalysts were obtained, in which the loading of Pt and Ni was controlled at 4 wt % and 0.3 wt %, respectively (molar ratio of Pt:Ni = 4:1). Subsequently, the fresh catalysts were reduced in flowing H_2 (30 mL/min) for 2 h at various temperatures. A pure Pt catalyst (4 wt % Pt/CB) was prepared by the same process.

Fresh and reduced Pt−Ni catalysts, 50 mg each, were washed in 20 mL dilute acid solutions (HCl or HNO_3, 2.5×10^{-3} mol/L). The concentrations of Pt and Ni ions in the leached solutions were analyzed by inductively coupled plasma atomic emission spectrometry (ICP-AES; Thermo Intrepid II). The acid leaching and the ICP measurements are employed to determine the distribution of Ni at the Pt−Ni NPs. The Pt−Ni NPs' size was characterized by using transmission electron microscopy (TEM; FEI Tecnai G2 Spirit, 120 kV).

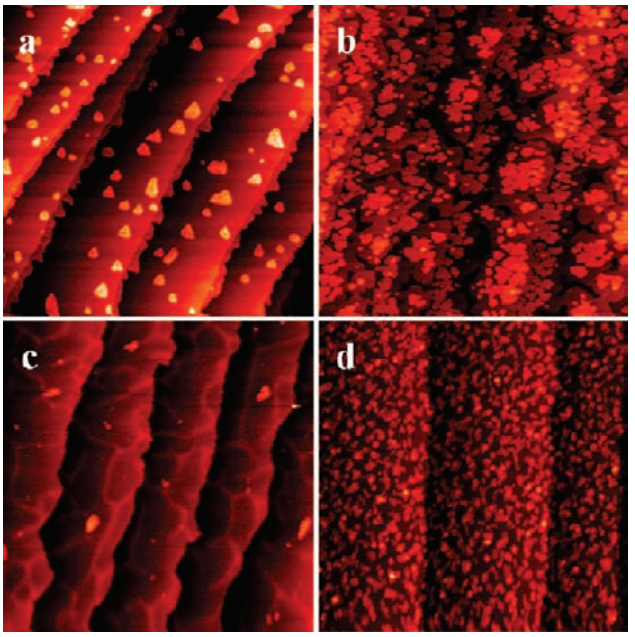

Figure 1. STM images of the surfaces of 0.16 ML Ni/Pt(111) (a), 1.3 ML Ni/Pt(111) (b), Pt/Ni/Pt(111) (c), and 0.16 ML NiO_{1-x}/Pt(111) (d). Conditions: (a) −0.350 V, 2.50 nA, 200 × 200 nm^2; (b) −0.302 V, 1.700 nA, 200 × 200 nm^2; (c) −0.275 V, 0.957 nA, 200 × 200 nm^2; (d) 2.365 V, 0.025 nA, 100 × 100 nm^2.

CO oxidation was carried out in a fixed-bed microreactor with four parallel reaction channels under identical conditions. The reaction gas consisted of 1% CO, 20% O_2, and 79% He, and the gas hourly space velocity was set at 30 000 mL g^{-1} h^{-1}. The tail gas was analyzed online using a multichannel mass spectrometer (Omnistar). For each reaction experiment, one of the four channels was empty and used as the blank, and a pure Pt catalyst (4 wt % Pt/CB) was put into another channel for comparison. CO conversion can be quantitatively determined on the basis of these reference data. Before reactions, all catalysts were reduced in flowing H_2 for 2 h at the specific temperature. After cooling to room temperature and purging the reactor with He, temperature-dependent CO oxidation was performed from room temperature to 200 °C.

X-ray absorption near-edge structure (XANES) spectra were measured at the BL14W1 beamline of the Shanghai Synchrotron Radiation Facility (SSRF). The Pt−Ni/CB catalysts reduced at various temperatures were characterized by Ni K-edge XANES in a fluorescence mode. Reduction of the fresh catalyst in flowing H_2 and subsequent CO oxidation of the reduced catalysts were investigated by XANES using an in situ reaction cell. For comparison, a 0.3 wt % Ni/CB sample was oxidized in air at 300 °C, and the Ni-edge XANES spectrum was recorded from this sample.

RESULTS AND DISCUSSION

Ni−Pt(111) Model Systems. Various Ni−Pt(111) surfaces were constructed in a well-defined way by using molecular beam epitaxy (MBE). First, Ni was epitaxially grown on Pt(111) under UHV conditions at room temperature. STM images show that 2D Ni islands with a coverage of 0.16 ML formed on the surface (Figure 1a). All the Pt(111) steps were decorated by the Ni islands, demonstrating the preferential growth of Ni at these defect sites. Ni islands with a size of 5−10 nm were also observed on the terraces. A height profile of the Ni islands reveals that all

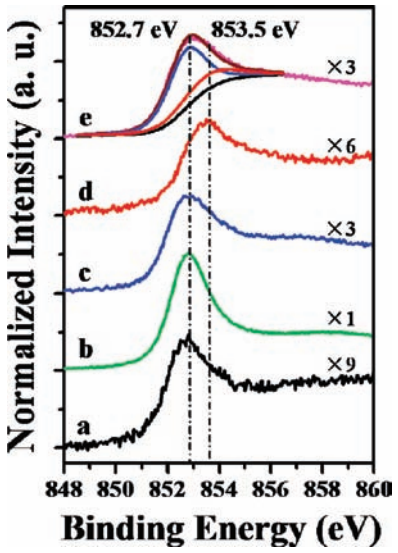

Figure 2. XPS Ni $2p_{3/2}$ spectra of the surfaces of 0.16 ML Ni/Pt(111) (a), 1.3 ML Ni/Pt(111) (b), Pt(111) with 1.3 ML subsurface Ni, Pt/Ni/Pt(111) (c), 0.16 ML NiO_{1-x}/Pt(111) (d), and 0.16 ML NiO_{1-x} on Pt/Ni/Pt(111) (e). To compare the line shapes, each spectrum has been multiplied by various numerical factors, which are indicated in the figure.

the islands are monolayer-dispersed, with thickness around 0.2 nm (Figure S1a). When the Ni coverage was increased to 1.3 ML, islands with thickness ranging from 1 to 3 ML were obtained (Figure 1b). In this case, the Pt(111) surface was fully covered by the Ni overlayers. The binding energy (BE) of XPS Ni $2p_{3/2}$ on the two surfaces is 852.7 eV, which indicates a metallic state of the deposited Ni overlayers (Figure 2a,b).

Second, the 1.3 ML Ni/Pt(111) surface was annealed at elevated temperatures in UHV. With increasing temperature, the ratio of the Ni 2p to the Pt 4f peak intensity kept decreasing (Figure S2). After heating at 800 K for 5 min, the Ni 2p intensity was attenuated by 67% (Figure 2c). At the same time, STM images show that Ni overlayers disappeared, and the surface presents a morphology similar to that of the clean Pt(111) (Figure 1c). However, a network of white lines can be observed on the terraces, which is characteristic for the Pt-skin structure containing TMs in the subsurface regions.[32,60,62,63] The above results confirm that UHV annealing of the Ni/Pt(111) surface at an appropriate temperature, e.g. 800 K, can induce inward diffusion of the surface Ni into the subsurface region, producing the Pt-skin surface, Pt/Ni/Pt(111).

Third, nickel oxide overlayers were prepared via evaporation of 0.16 ML Ni onto Pt(111) at room temperature in 1.3×10^{-6} mbar O_2, similar to the procedure used to prepare FeO/Pt(111) surfaces.[61] The XPS Ni $2p_{3/2}$ spectrum recorded from the surface peaked at 853.5 eV, close to the Ni^{2+} state (Figure 2d).[64,65] Meanwhile, the ratio of O 1s to Ni 2p peak area was less than that of a fully oxidized NiO layer grown on highly oriented pyrolytic graphite (HOPG) (Figure S3). Thus, the obtained Ni oxide overlayers are oxygen-deficient and can be denoted as NiO_{1-x}/Pt(111) ($x < 1$). STM images indicate that the formed NiO_{1-x} nanoislands are highly dispersed on the Pt(111) surface (Figure 1d). More importantly, the oxide nanostructures have monolayer thickness (Figure S1b), similar to NiO nanostructures grown on Pt(111)[66] and Pd(100).[67] It should be noted that, under the same deposition conditions, 3D NiO islands were obtained on the HOPG surface (Figure S4). Therefore, it can be concluded that the interface confinement effect between oxide overlayers and metal substrates also plays a critical role in stabilization of the 2D NiO nanoislands. The interaction between TM oxides and noble metals plays an important role in the interface effect.[46,68−70]

The reactivity of the above-mentioned surfaces toward CO oxidation was investigated by using in situ UPS.[46,60] All the surfaces were first saturated with CO via adsorption of 10 L CO at room temperature. The CO presaturated surfaces were exposed to 4.0×10^{-8} mbar O_2 at room temperature, and UPS He II spectra were acquired simultaneously at one spectrum per minute. The $5\sigma + 1\pi$ and 4σ molecular orbits of CO adsorbed on Pt(111) are the main features in the UPS spectra, located at 9.4 and 11.8 eV, respectively.[60,71,72] The evolution of the peak intensity with reaction time was used to characterize the surface reactivity.

On the Pt(111) surface, the intensity of the two CO peaks does not change, even after exposing the surface to 4.0×10^{-8} mbar O_2 for 0.5 h (Figure 3a). This result is not unexpected, considering the well-known CO poisoning effect on pure Pt surfaces.[73] Only at elevated temperatures may CO desorption occur, which leaves available surface sites for O_2 adsorption and helps CO oxidation.

The Pt-skin surface, Pt/Ni/Pt(111), presents reactivity similar to that of Pt(111). As shown in Figure 3b, no obvious decrease in CO intensity can be observed in the time-elapsed UPS spectra. Mavrikakis and co-workers calculated the activation energy for O_2 dissociation on Pt(111) and Pt-skin surfaces with subsurface TMs.[12,44,45] They found that O_2 activation on the Pt-skin surface becomes more energetically demanding, for example 0.77 eV on Pt(111) and 0.93 eV on Pt-skin with subsurface Co. The lost reactivity of the Pt-skin surfaces to O_2 activation has been attributed to both strain and ligand effects.[12] We also studied O_2 dissociation on Pt(111) and a Pt-skin layer on Pt_3Ni, and a similar trend (0.71 eV on Pt(111) vs 0.97 eV on the Pt-skin) was found.[51,74] On the other hand, adsorption of CO, H, O, and O_2 on Pt-skin surfaces is weakened by the subsurface TMs,[9,10,32,51−53,60] but the destabilization occurs with a similar magnitude.[44,51] For example, binding energies of CO and O_2 on a Pt-skin with subsurface Ru are −1.25 and −0.26 eV, respectively, compared to −1.82 eV/CO and −0.65 eV/O_2 on Pt(111).[44] On the basis of these arguments, the Pt-skin surfaces are still poisoned by CO, and the CO oxidation is limited by O_2 activation in the low-temperature regime. Therefore, it can be understood that the Pt-skin surface does not present much higher reactivity toward CO oxidation than Pt(111).

It should be noted that the Pt/Ni/Pt(111) surface is quite stable during the CO oxidation process. We performed XPS measurement of the Pt-skin surface after CO oxidation and exposure to 4.0×10^{-8} mbar O_2 up to 391 K, and no change in the Ni 2p spectra was observed (Figure S5). Chen and co-workers studied outward diffusion of Ni at Pt surfaces. The activation energy for the Ni diffusion was determined to be 17 ± 1 kcal/mol.[75] It is thus expected that Ni diffusion onto the surface is kinetically limited near room temperature.

Over the 0.16 ML Ni/Pt(111) surface, CO can react with O_2 slowly. Figure 3c shows that the intensity of the two CO features decreases gradually with O_2 exposure time. CO has been completely reacted away in 20 min. After the reaction, XPS Ni $2p_{3/2}$ BE shifts from 852.7 to 853.4 eV (Figure S6). This result indicates that the surface Ni is prone to be oxidized in the

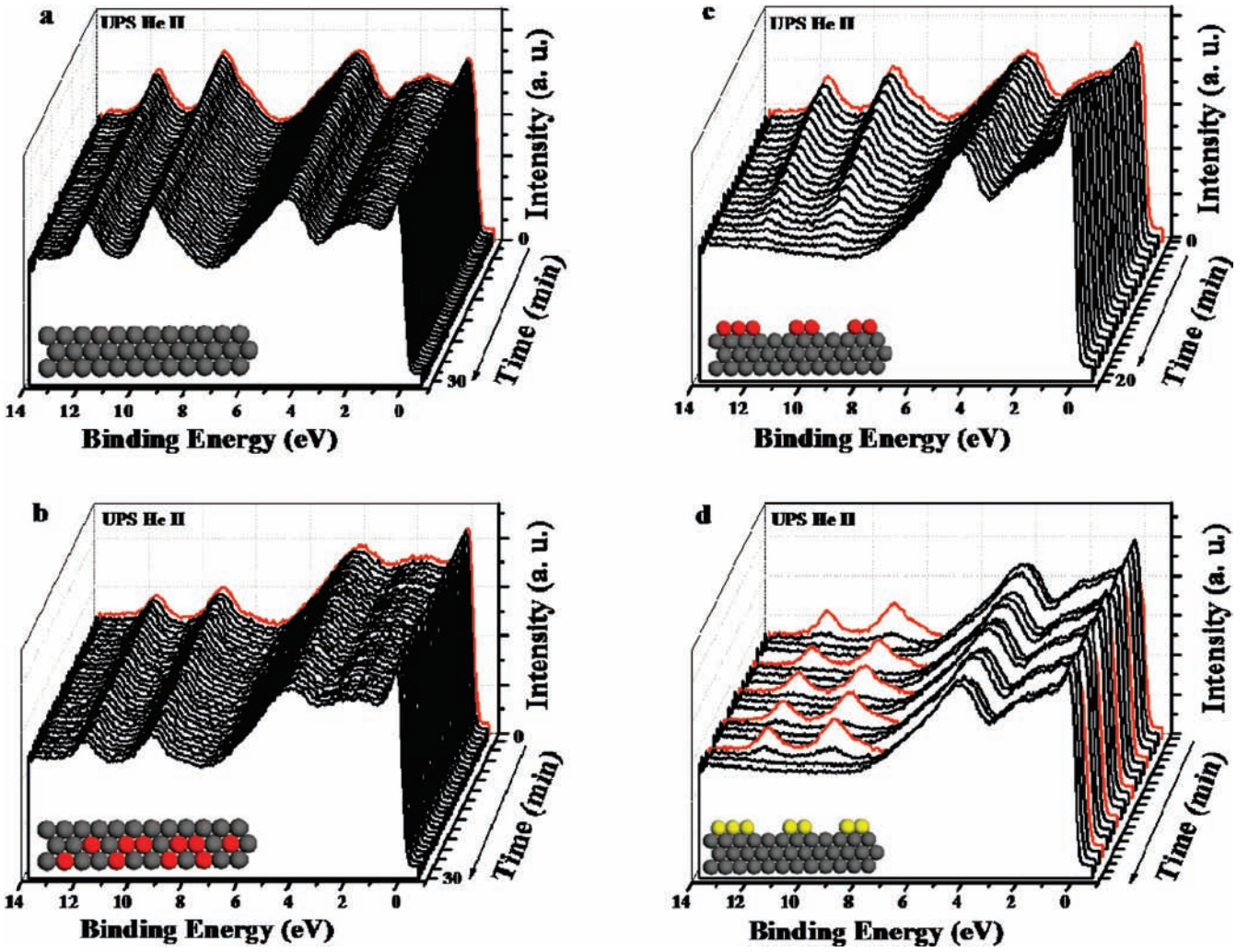

Figure 3. In situ He II UPS spectra recorded from the CO-presaturated surfaces exposed to 4.0×10^{-8} mbar O_2 at room temperature: (a) the bare Pt(111) surface; (b) the Pt(111) with 1.3 ML subsurface Ni, Pt/Ni/Pt(111); (c) the 0.16 ML Ni/Pt(111) surface; (d) the 0.16 ML NiO_{1-x}/Pt(111) surface. The red line is the onset of the reaction. Inset: gray, Pt; red, Ni; yellow, NiO_{1-x}.

oxidative atmosphere. As discussed below, the formed oxidized Ni structure may contribute to the observed CO oxidation activity.

Much higher reactivity was observed on the NiO_{1-x}/Pt(111) surface. Figure 3d demonstrates that the preadsorbed CO can be eliminated in 2 min in 4.0×10^{-8} mbar O_2. Furthermore, the reaction was repeated several times, and the surface reactivity did not change with the reaction cycle. As established previously, coordinatively unsaturated cations confined at interfaces between nanostructured oxides and metal substrates are highly active for activation of O_2.[46] We suggest that the high reactivity of the NiO_{1-x}/Pt(111) surface can be attributed to the presence of 2D NiO_{1-x} nanoislands and coordinatively unsaturated Ni atoms at the island edges as well.

Su et al. studied the effect of subsurface Ni on the elementary reaction of CO with O on the Pt-skin surfaces using density functional theory (DFT) calculation. They showed that the presence of subsurface Ni atoms lowers the activation energy for CO + O reaction by a few tenths of an electronvolt.[51] Nilekar et al. also calculated CO + O activation energies on a layer of Pt-skin placed on top of three-layer slabs of Ru(0001), Rh(111), Pd(111), and Ir(111), and all the values were smaller than that on the Pt(111) surface, e.g., 0.79 eV on Pt(111) vs 0.41 eV on Pt*/Ru(0001).[44,45] Subsurface TMs weaken the adsorption of reactants of CO and O on metals, which results in smaller reaction barriers and substantial enhancement of the elementary reaction of CO oxidation with O.[51,76] Obviously, the enhancement effect becomes activated only if atomic O species are available. As discussed above, O_2 activation is still the limiting step for CO oxidation on the Pt-skin surfaces; thus, the subsurface enhancement effect has not been observed (Figure 3b). Considering that surface TM oxides help to facilitate dissociation of O_2,[46] we expect subsurface TMs may enhance the surface reactivity by working together with surface TM oxides.

To shed light on the synergistic effect from the subsurface Ni and surface NiO_{1-x} structures, we built another model system, denoted as NiO_{1-x}/Pt/Ni/Pt(111). This surface was prepared by evaporation of 0.16 ML Ni onto the Pt-skin surface at room temperature in 1.3×10^{-6} mbar O_2. XPS measurement confirms that Ni at this surface presents both oxidized and metallic states (Figure 2e). Moreover, the Ni oxide deposited on the Pt-skin surface presents island dispersion and monolayer thickness similar to those on the Pt(111) surface (Figure S1c).

On the NiO_{1-x}/Pt/Ni/Pt(111) surface, CO can be reacted away in 2 min in 4.0×10^{-8} mbar O_2 at room temperature.

dx.doi.org/10.1021/ja109483a | J. Am. Chem. Soc. 2011, 133, 1978–1986

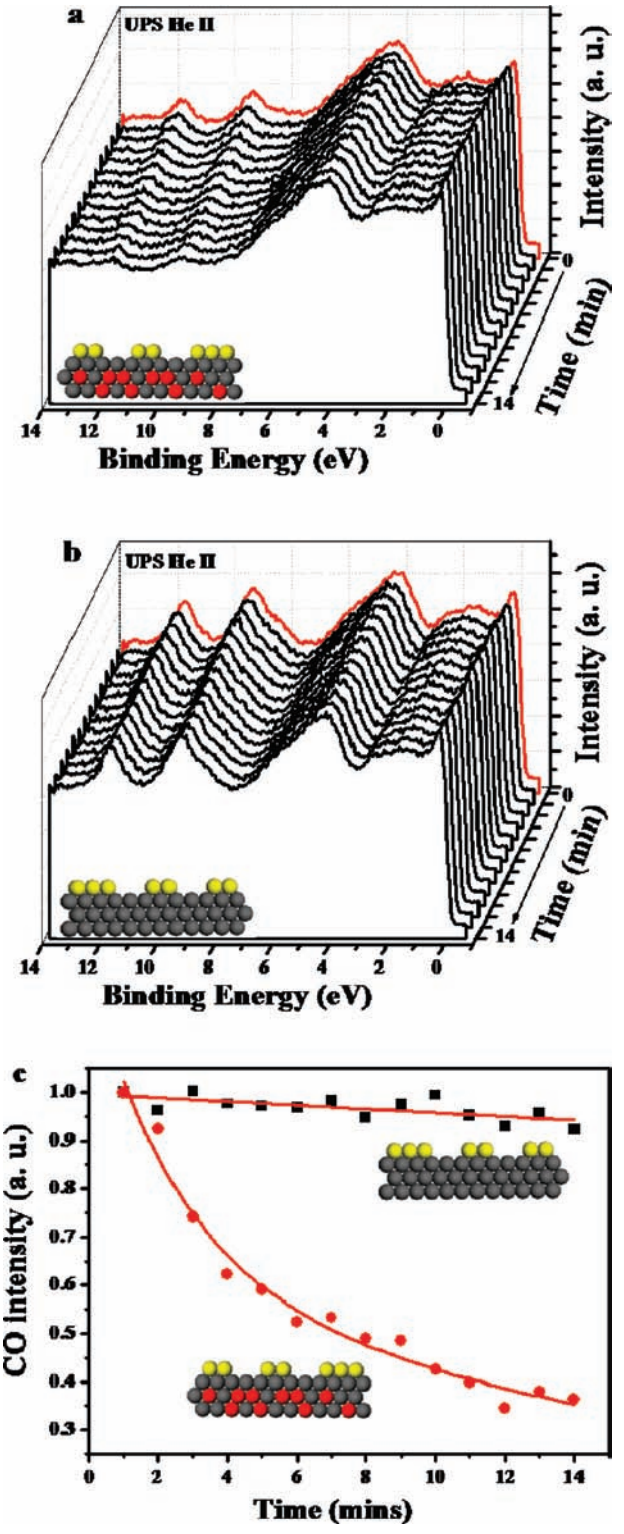

Figure 4. In situ He II UPS spectra recorded from the CO presaturated surfaces exposed to 4.0 × 10^{-8} mbar O_2 at 220 K: (a) the 0.16 ML NiO_{1-x}/Pt/Ni/Pt(111) surface and (b) the 0.16 ML NiO_{1-x}/Pt-(111)surface. (c) Plots of the CO 4σ peak area as a function of O_2 exposure time on the two surfaces.

In order to see the difference in surface reactivity between the NiO_{1-x}/Pt/Ni/Pt(111) and NiO_{1-x}/Pt(111) surfaces, we carried out the CO oxidation reaction at 220 K. Under this

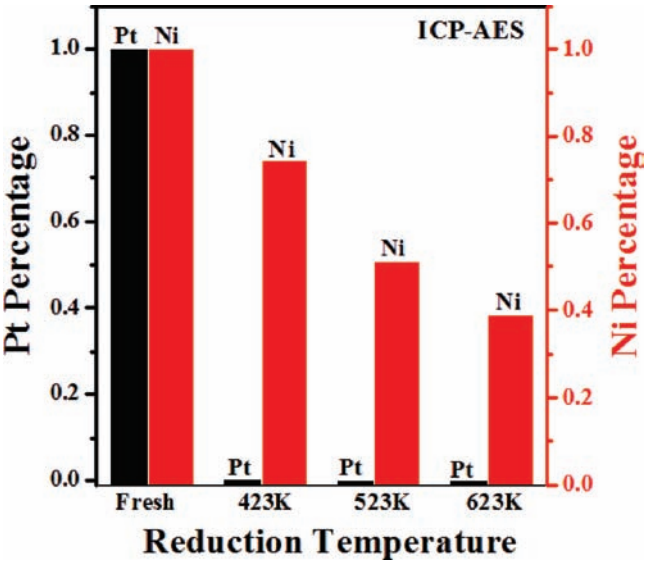

Figure 5. Concentrations of Pt and Ni ions in the leached acid solutions from the fresh PtNi/CB catalyst and the catalysts reduced at 423, 523, and 623 K. The concentrations were measured by ICP-AES, and the values from the fresh catalysts were normalized to 100%.

condition, CO oxidation did not happen on the NiO_{1-x}/Pt(111) surface, while most of the CO was removed by O_2 in 14 min on the NiO_{1-x}/Pt/Ni/Pt(111) surface (Figure 4). The in situ reaction data show that the sandwich NiO_{1-x}/Pt/Ni/Pt(111)surface has the highest reactivity to CO oxidation among the Ni−Pt-(111) surfaces studied.

Supported Pt−Ni Catalysts. Pt−Ni practical catalysts supported on carbon black, PtNi/CB, were prepared by wetness co-impregnation and reduced in H_2. Since Pt precursors can be reduced by H_2 more easily than precursors of 3d TMs, the initial structural configuration of Pt-3d-TM catalysts prepared by the co-impregnation and co-reduction process should be Pt NPs decorated by 3d-TM overlayers.[77] On the other hand, inward diffusion of surface 3d-TMs into the subsurface or even bulk regions of Pt crystals may happen upon heating in UHV or reductive atmospheres (Figure S2).[10,56,60,62,78,79] Accordingly, the surface structure of the PtNi/CB catalysts can be simply controlled by reduction in H_2. For this purpose, our PtNi/CB catalysts were reduced in H_2 for 2 h at 423, 523, and 623 K, respectively.

Acid leaching of Pt-3d-TM alloy crystals or NPs can remove the surface TM atoms but leave those in the bulk unchanged, producing the Pt-skin or Pt-skeleton structures.[14,17,20,80−82] A fresh PtNi/CB sample without reduction was treated by the leaching process. In this sample, all Ni and Pt ions were completely washed away. The measured Ni and Pt concentrations are included in Figure 5 as a reference. After reduction, ICP data show that only a trace amount of Pt is detected, which indicates that the Pt precursor is fully reduced under all the treatment conditions (Figure 5). In contrast, there is always a certain amount of Ni in the leached solutions. In the PtNi/CB sample reduced at 423 K, more than 75% Ni has been dissolved away, while only one-third of Ni can be washed from the catalysts in the case of reduction at 623 K. Accordingly, we can conclude that a large part of Ni is still located at the outside of the Pt−Ni NPs reduced at 423 K. In contrast, reduction at 623 K drives diffusion of most Ni atoms into the NPs, and the formed Pt-skin

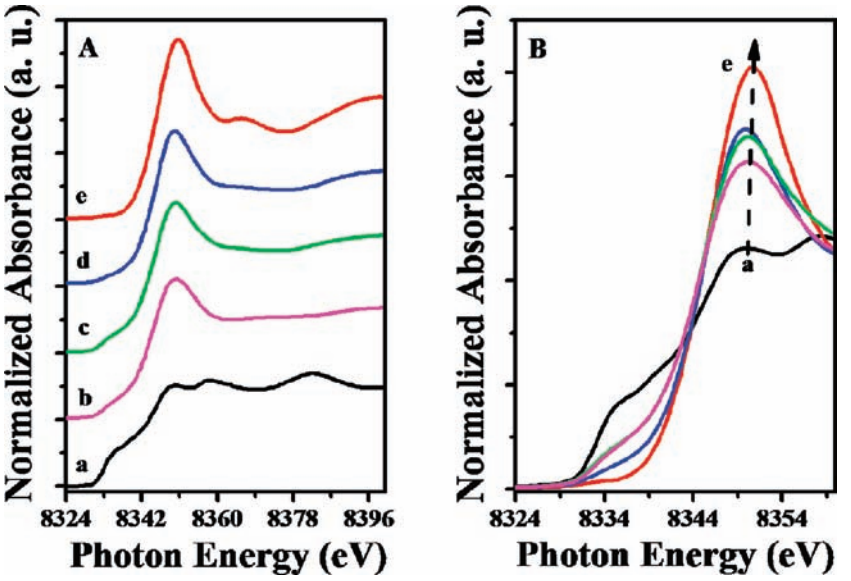

Figure 6. (A) Ni K-edge XANES spectra acquired from different PtNi samples: (a) Ni foil; (b) PtNi/CB catalysts reduced at 623 K for 2 h and then exposed to air at room temperature; (c) PtNi/CB catalysts reduced at 523 K for 2 h and then exposed to air at room temperature; (d) PtNi/CB catalysts reduced at 423 K for 2 h and then exposed to air at room temperature; (e) NiO/CB catalysts. (B) Zoomed white line peaks in (A).

surface prevents Ni inside the particles from leaching. In between, e.g. around 523 K, half of the Ni is present outside of the NPs, while the rest remains inside.

Ni K-edge XANES spectra were acquired from the PtNi/CB samples and used to determine the chemical state of the Ni species. Reduction of the sample in flowing H_2 was monitored by in situ XANES. At 423 K, the spectrum was already similar to the Ni foil spectrum (Figure S7), which indicates that Ni is completely reduced to the metallic state under this reduction condition. The reduction of Ni species in the Pt−Ni catalysts at lower temperatures is facilitated by the promoting effect of Pt.[41,83]

The samples reduced under different conditions were studied by XANES in air, and Ni K-edge structures are shown in Figure 6. For comparison, the spectrum from the NiO/CB sample is also included. The Ni K-edge structure from the sample reduced at 423 K resembles that of the NiO/CB, with the high intensity of the white line caused by the Ni−O interaction.[56] As the reduction temperature increases, the intensity of the white line decreases, and the spectra look more like the Ni foil spectrum. Furthermore, the peak position of the white line also shifts to lower energy. All these results suggest the conversion from Ni^{2+}-rich to Ni^{0+}-rich state at the Pt−Ni NPs when the reduction temperature is increased.

The XANES results further support the structural configurations of the Pt−Ni NPs as derived from the leaching/ICP experiments, which indicate that the distribution of Ni at the Pt−Ni NPs can be simply modulated by reduction in H_2. At low reduction temperature, e.g. 423 K, most Ni species are still outside of the particles and oxidized upon exposure to air at room temperature. The remaining Ni atoms diffusing into the NPs are protected from oxidation by air. Upon reduction at 623 K, most of the Ni atoms diffuse into the subsurface or bulk regions of the NPs, which remain metallic in air. The observed metallic state of subsurface Ni species in the supported NPs by XANES also confirms the high stability of Pt-skin surfaces when exposed to an oxidative atmosphere at relatively low temperature, e.g. 20% O_2 in air at room temperature.

The reactivity to CO oxidation (1% CO, 20% O_2, He balance) was studied over the PtNi/CB samples reduced in H_2 at various

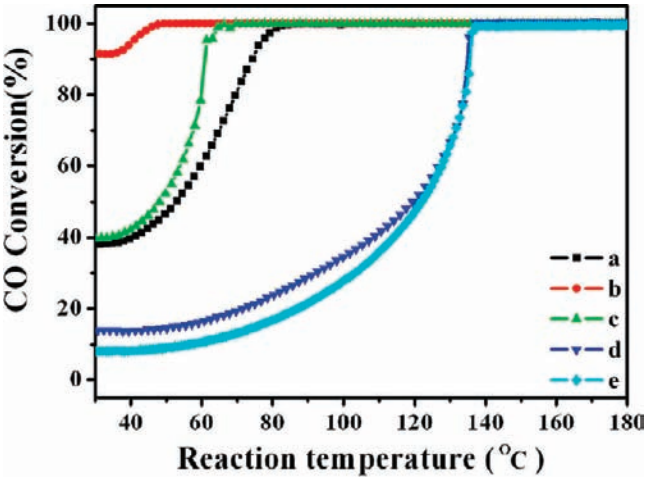

Figure 7. Temperature-dependent CO conversion in the CO oxidation over the PtNi/CB catalysts reduced at (a) 423, (b) 523, and (c) 623 K, respectively; For comparison, the results on the Pt/CB catalyst (d) and the leached PtNi/CB catalyst (e) are also included.

temperatures. The dependence of CO conversion on the reaction temperature is shown in Figure 7. It is interesting to see that the best reactivity is observed on the PtNi/CB sample reduced at an intermediate temperature, 523 K. With this catalyst, 100% CO conversion occurs at 320 K. By contrast, the catalysts reduced at 423 or 623 K demonstrate worse performance, in which 100% CO conversion takes place at 356 and 340 K, respectively. Moreover, CO conversion of the two catalysts at room temperature is much less than that reduced at 523 K. Reaction data from the Pt/CB catalyst (4 wt %) are included in Figure 7 for comparison. It can be seen that the Pt/CB catalyst has much lower CO oxidation activity than the Pt−Ni catalysts, and only at 410 K does complete CO oxidation happen. The Pt/CB catalyst was reduced in H_2 at the three temperatures, and no effect of the reduction temperature on the activity was observed. It is known that supported metal NPs may sinter at elevated temperatures.

dx.doi.org/10.1021/ja109483a |*J. Am. Chem. Soc.* 2011, 133, 1978–1986

The PtNi/CB samples reduced at 423 and 623 K were investigated by TEM (Figure S8). Both samples showed similar catalyst size distribution in the range of 2−6 nm. Therefore, the sintering effect can be excluded within this temperature range (between 423 and 623 K). On the basis of these results, we can conclude that the effect of the reduction temperature on the reactivity of the PtNi/CB catalysts is mainly due to the variation of the surface structure at the PtNi NPs.

Architecture of Pt−Ni Catalysts for CO Oxidation. Using surface science experiments, we show that the reactivity of Ni−Pt(111) surfaces to CO oxidation increases in the sequence of Pt(111) < Pt/Ni/Pt(111) < Ni/Pt(111) < NiO_{1-x}/Pt(111) < NiO_{1-x}/Pt/Ni/Pt(111). On the basis of the results, two important factors in CO oxidation over the Ni−Pt(111) surfaces can be derived. First, the presence of highly dispersed NiO_{1-x} nanostructures on Pt surfaces plays a critical role in dissociative adsorption of O_2, which helps to alleviate CO poisoning on Pt and produces atomic O species. Second, subsurface Ni enhances the elementary reaction of CO oxidation with O. The CO oxidation with O_2 can be promoted by the subsurface Ni species in case that atomic O species are produced by the surface NiO_{1-x} nanostructures. It is reasonable to expect that the sandwich NiO_{1-x}/Pt/Ni/Pt(111) surface demonstrates the highest reactivity.

For the supported Pt−Ni NPs, the XANES and leaching experiments clearly show that location of Ni at the Pt−Ni NPs can be simply controlled by reduction in H_2. The surface Ni gets oxidized when exposed to oxidative atmospheres, e.g. 4×10^{-8} mbar O_2 (Figure S6), air (Figure 6), and CO oxidation gases (1% CO, 20% O_2, He balance, Figure S7), while the subsurface Ni remains metallic near room temperature under oxidizing conditions due to the kinetic limit of outward diffusion of Ni. With the reduction temperature at 423 K, most of the Ni species are still outside of the NPs, and the surface structure of the Pt−Ni NPs resembles the NiO_{1-x}/Pt(111) surface. High-temperature reduction, e.g. 623 K, produces the Pt-skin structure, like the Pt/Ni/Pt(111) model system. At an intermediate temperature of 523 K, around half of the Ni is outside and the rest is inside of the NPs. Under the oxidation condition, this catalyst contains both surface Ni oxide and subsurface Ni atoms, which presents the sandwich surface structure as the NiO_{1-x}/Pt/Ni/Pt(111) model surface.

The highest reactivity of the sandwich PtNi/CB catalyst to CO oxidation among the supported Pt−Ni catalysts investigated here (Figure 7), and the highly active NiO_{1-x}/Pt/Ni/Pt(111) surface compared to other Ni−Pt(111) model surfaces (Figure 4), suggest the important role of both surface Ni oxides and subsurface Ni in the CO oxidation. As discussed above, the surface Ni oxide monolayer nanoislands contain coordinatively unsaturated cations at the island edges, which provide active sites for O_2 dissociative adsorption. On the other hand, the subsurface Ni atoms enhance the elementary reaction of CO oxidation, with atomic O species produced at the edges of the surface oxide islands. Since the Pt-skin surface was produced by the surface segregation process, the ligand effect seems to be more critical than the strain effect in the observed subsurface enhancement.[52] The synergetic effect of surface and subsurface Ni species at the Pt−Ni catalysts for the CO oxidation reaction is illustrated by Scheme 1.

To further confirm this synergetic effect, CO oxidation was performed on a leached PtNi/CB catalyst. The fresh PtNi/CB sample was reduced at 523 K to form the highly active sandwich structure. It was then leached in the acid solution to remove the surface Ni species. After activation in H_2 at 423 K, a temperature-dependent reaction was performed on the catalyst. The reaction data indicate that the reactivity of the leached sample is similar to that of the Pt/CB catalyst (Figure 7). Although ICP data show that the leaching washes only half of the Ni from the Pt−Ni NPs (Figure 5), removal of surface Ni species and formation of the Pt-skeleton structure lower the surface reactivity significantly.

Scheme 1. Synergetic Effect of Surface Ni Oxide and Subsurface Ni Species at Pt−Ni Catalysts on the CO Oxidation[a]

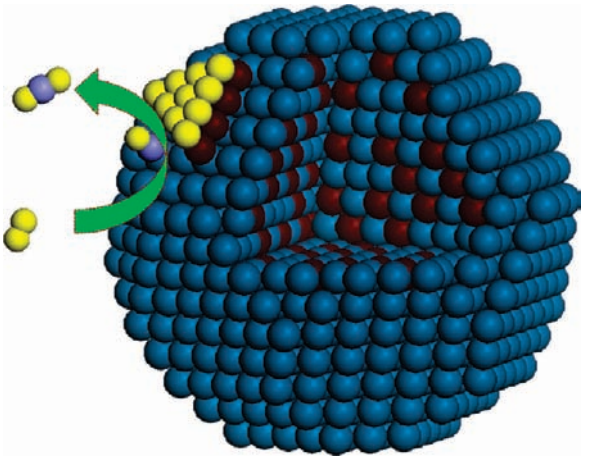

[a] Surface Ni oxide structure activates dissociation of O_2 and subsurface Ni atoms promote CO reaction with O. O, yellow; Ni, brown; Pt, cyan; C, light blue.

The results from the Ni−Pt(111) model systems and the supported Pt−Ni catalysts are consistent with each other, and both of them illustrate the synergetic effect in Pt−Ni catalytic systems. Although the surface structure of the supported catalyst NPs is complex, in particular for the multicomponent catalysts, a bridge between model systems and practical catalysts made in this work helps to understand the reaction mechanism at the microscopic scale and to construct highly efficient practical nanocatalysts.[84] Furthermore, our work demonstrates that activation in H_2 is a simple but effective route to manipulate the surface architecture of multicomponent catalysts and produce the active sandwich Pt−Ni catalysts. Considering that activation of powdered catalysts in H_2 is the most frequently used pretreatment, the sandwich Pt−TM catalysts produced by the reduction process should be generally present in many Pt−TM systems but are often ignored. Therefore, we expect that the synergetic catalytic mechanism may be widely applied in other Pt-based bimetallic catalytic systems.

CONCLUSIONS

A well-defined sandwich Ni−Pt(111) surface consisting of both surface 2D NiO_{1-x} nanoislands and subsurface Ni atoms presents high reactivity to the CO oxidation. The surface NiO_{1-x} nanoislands provide the active edge sites for O_2 dissociative adsorption, producing atomic O species, while the subsurface Ni atoms enhance the elementary reaction of CO oxidation with O. A similar sandwich structure was constructed at Pt−Ni practical catalysts via a simple reduction process. Upon heating the supported Pt−Ni NPs in H_2 at an intermediate temperature of 523 K, half of the Ni remains outside of the NPs and the rest diffuses to subsurface regions, which transform to surface Ni oxide and

subsurface Ni, respectively, after exposure to an oxidative atmosphere. The synergetic effect of the surface and subsurface Ni species in this supported Pt−Ni catalyst results in high surface reactivity as well. The bridge between model systems and real catalysts helps to illustrate the bimetallic catalytic mechanism and to fabricate highly efficient practical bimetallic catalysts.

■ ASSOCIATED CONTENT

Supporting Information. Figures S1−S8. This material is available free of charge via the Internet at http://pubs.acs.org.

■ AUTHOR INFORMATION

Corresponding Author
qfu@dicp.ac.cn; xhbao@dicp.ac.cn

■ ACKNOWLEDGMENT

This work was financially supported by the National Natural Science Foundation of China (Nos. 20733008, 2087314, and 11079005), Ministry of Science and Technology of China, Chinese Academy of Sciences ("Bairen" program), and the Science and Technology Commission of Shanghai Municipality of China (No. 09JC1417100). We thank Prof. Weixue Li and Dr. Chuanfu Wang for fruitful discussions.

■ REFERENCES

(1) Rodriguez, J. A.; Goodman, D. W. *Science* **1992**, *257*, 897–903.
(2) Rodriguez, J. A. *Surf. Sci. Rep.* **1996**, *24*, 225–287.
(3) Besenbacher, F.; Chorkendorff, I.; Clausen, B. S.; Hammer, B.; Molenbroek, A. M.; Norskov, J. K.; Stensgaard, I. *Science* **1998**, *279*, 1913–1915.
(4) Greeley, J.; Jaramillo, T. F.; Bonde, J.; Chorkendorff, I. B.; Norskov, J. K. *Nat. Mater.* **2006**, *5*, 909–913.
(5) Chen, M. S.; Kumar, D.; Yi, C. W.; Goodman, D. W. *Science* **2005**, *310*, 291–293.
(6) Enache, D. I.; Edwards, J. K.; Landon, P.; Solsona-Espriu, B.; Carley, A. F.; Herzing, A. A.; Watanabe, M.; Kiely, C. J.; Knight, D. W.; Hutchings, G. J. *Science* **2006**, *311*, 362–365.
(7) Zhang, J.; Sasaki, K.; Sutter, E.; Adzic, R. R. *Science* **2007**, *315*, 220–222.
(8) Markovic, N. M.; Ross, P. N. *Surf. Sci. Rep.* **2002**, *45*, 121–229.
(9) Stamenkovic, V. R.; Fowler, B.; Mun, B. S.; Wang, G. F.; Ross, P. N.; Lucas, C. A.; Markovic, N. M. *Science* **2007**, *315*, 493–497.
(10) Chen, J. G.; Menning, C. A.; Zellner, M. B. *Surf. Sci. Rep.* **2008**, *63*, 201–254.
(11) Hansgen, D. A.; Vlachos, D. G.; Chen, J. G. G. *Nature Chem.* **2010**, *2*, 484–489.
(12) Xu, Y.; Ruban, A. V.; Mavrikakis, M. *J. Am. Chem. Soc.* **2004**, *126*, 4717–4725.
(13) Arenz, M.; Mayrhofer, K. J. J.; Stamenkovic, V.; Blizanac, B. B.; Tomoyuki, T.; Ross, P. N.; Markovic, N. M. *J. Am. Chem. Soc.* **2005**, *127*, 6819–6829.
(14) Stamenkovic, V. R.; Mun, B. S.; Mayrhofer, K. J. J.; Ross, P. N.; Markovic, N. M. *J. Am. Chem. Soc.* **2006**, *128*, 8813–8819.
(15) Nilekar, A. U.; Mavrikakis, M. *Surf. Sci.* **2008**, *602*, L89–L94.
(16) Koh, S.; Leisch, J.; Toney, M. F.; Strasser, P. *J. Phys. Chem. C* **2007**, *111*, 3744–3752.
(17) Koh, S.; Strasser, P. *J. Am. Chem. Soc.* **2007**, *129*, 12624–12625.
(18) Chen, S.; Ferreira, P. J.; Sheng, W. C.; Yabuuchi, N.; Allard, L. F.; Shao-Horn, Y. *J. Am. Chem. Soc.* **2008**, *130*, 13818–13819.
(19) Chen, S.; Sheng, W. C.; Yabuuchi, N.; Ferreira, P. J.; Allard, L. F.; Shao-Horn, Y. *J. Phys. Chem. C* **2009**, *113*, 1109–1125.
(20) Mayrhofer, K. J. J.; Juhart, V.; Hartl, K.; Hanzlik, M.; Arenz, M. *Angew. Chem., Int. Ed.* **2009**, *48*, 3529–3531.
(21) Mayrhofer, K. J. J.; Hartl, K.; Juhart, V.; Arenz, M. *J. Am. Chem. Soc.* **2009**, *131*, 16348–16349.
(22) Kim, J.; Lee, Y.; Sun, S. H. *J. Am. Chem. Soc.* **2010**, *132*, 4996–4997.
(23) Sasaki, K.; Naohara, H.; Cai, Y.; Choi, Y. M.; Liu, P.; Vukmirovic, M. B.; Wang, J. X.; Adzic, R. R. *Angew. Chem., Int. Ed.* **2010**, *49*, 8602–8607.
(24) Hwu, H. H.; Eng, J.; Chen, J. G. G. *J. Am. Chem. Soc.* **2002**, *124*, 702–709.
(25) Murillo, L. E.; Goda, A. M.; Chen, J. G. *J. Am. Chem. Soc.* **2007**, *129*, 7101–7105.
(26) Hirschl, R.; Delbecq, F.; Sautet, P.; Hafner, J. *J. Catal.* **2003**, *217*, 354–366.
(27) Delbecq, F.; Sautet, P. *J. Catal.* **2003**, *220*, 115–126.
(28) Haubrich, J.; Loffreda, D.; Delbecq, F.; Sautet, P.; Jugnet, Y.; Krupski, A.; Becker, C.; Wandelt, K. *J. Phys. Chem. C* **2008**, *112*, 3701–3718.
(29) Haubrich, J.; Loffreda, D.; Delbecq, F.; Sautet, P.; Krupski, A.; Becker, C.; Wandelt, K. *J. Phys. Chem. C* **2009**, *113*, 13947–13967.
(30) Haubrich, J.; Loffreda, D.; Delbecq, F.; Sautet, P.; Jugnet, Y.; Becker, C.; Wandelt, K. *J. Phys. Chem. C* **2010**, *114*, 1073–1084.
(31) Liu, D. X.; Lopez-De Jesus, Y. M.; Monnier, J. R.; Williams, C. T. *J. Catal.* **2010**, *269*, 376–387.
(32) Knudsen, J.; Nilekar, A. U.; Vang, R. T.; Schnadt, J.; Kunkes, E. L.; Dumesic, J. A.; Mavrikakis, M.; Besenbacher, F. *J. Am. Chem. Soc.* **2007**, *129*, 6485–6490.
(33) Margitfalvi, J. L.; Borbath, I.; Hegedus, M.; Tfirst, E.; Gobolos, S.; Lazar, K. *J. Catal.* **2000**, *196*, 200–204.
(34) Margitfalvi, J. L.; Borbath, I.; Lazar, K.; Tfirst, E.; Szegedi, A.; Hegedus, M.; Gobolos, S. *J. Catal.* **2001**, *203*, 94–103.
(35) Liu, X. S.; Korotkikh, O.; Farrauto, R. *Appl. Catal. A-Gen.* **2002**, *226*, 293–303.
(36) Tanaka, K.; Moro-oka, Y.; Ishigure, K.; Yajima, T.; Okabe, Y.; Kato, Y.; Hamano, H.; Sekiya, S.; Tanaka, H.; Matsumoto, Y.; Koinuma, H.; He, H.; Zhang, C. B.; Feng, Q. C. *Catal. Lett.* **2004**, *92*, 115–121.
(37) Tanaka, K. I.; Shou, M.; He, H.; Shi, X. Y. *Catal. Lett.* **2006**, *110*, 185–190.
(38) Kotobuki, M.; Watanabe, A.; Uchida, H.; Yamashita, H.; Watanabe, M. *J. Catal.* **2005**, *236*, 262–269.
(39) Sirijaruphan, A.; Goodwin, J. G., Jr.; Rice, R. W. *J. Catal.* **2004**, *224*, 304–313.
(40) Siani, A.; Captain, B.; Alexeev, O. S.; Stafyla, E.; Hungria, A. B.; Midgley, P. A.; Thomas, J. M.; Adams, R. D.; Amiridis, M. D. *Langmuir* **2006**, *22*, 5160–5167.
(41) Ko, E. Y.; Park, E. D.; Seo, K. W.; Lee, H. C.; Lee, D.; Kim, S. *Catal. Lett.* **2006**, *110*, 275–279.
(42) Ko, E. Y.; Park, E. D.; Lee, H. C.; Lee, D.; Kim, S. *Angew. Chem., Int. Ed.* **2007**, *46*, 734–737.
(43) Alayoglu, S.; Eichhorn, B. *J. Am. Chem. Soc.* **2008**, *130*, 17479–17486.
(44) Alayoglu, S.; Nilekar, A. U.; Mavrikakis, M.; Eichhorn, B. *Nat. Mater.* **2008**, *7*, 333–338.
(45) Nilekar, A. U.; Alayoglu, S.; Eichhorn, B.; Mavrikakis, M. *J. Am. Chem. Soc.* **2010**, *132*, 7418–7428.
(46) Fu, Q.; Li, W. X.; Yao, Y. X.; Liu, H. Y.; Su, H. Y.; Ma, D.; Gu, X. K.; Chen, L. M.; Wang, Z.; Zhang, H.; Wang, B.; Bao, X. H. *Science* **2010**, *328*, 1141–1144.
(47) Sun, Y. N.; Giordano, L.; Goniakowski, J.; Lewandowski, M.; Qin, Z. H.; Noguera, C.; Shaikhutdinov, S.; Pacchioni, G.; Freund, H. J. *Angew. Chem., Int. Ed.* **2010**, *49*, 4418–4421.
(48) Scott, F. J.; Roth, C.; Ramaker, D. E. *J. Phys. Chem. C* **2007**, *111*, 11403–11413.
(49) Scott, F. J.; Mukerjee, S.; Ramaker, D. E. *J. Phys. Chem. C* **2010**, *114*, 442–453.

(50) Liu, Z. F.; Jackson, G. S.; Eichhorn, B. W. *Angew. Chem., Int. Ed.* **2010**, *49*, 3173–3176.
(51) Su, H. Y.; Bao, X. H.; Li, W. X. *J. Chem. Phys.* **2008**, *128*, 194707.
(52) Kitchin, J. R.; Norskov, J. K.; Barteau, M. A.; Chen, J. G. *J. Chem. Phys.* **2004**, *120*, 10240–10246.
(53) Stamenkovic, V.; Mun, B. S.; Mayrhofer, K. J. J.; Ross, P. N.; Markovic, N. M.; Rossmeisl, J.; Greeley, J.; Norskov, J. K. *Angew. Chem., Int. Ed.* **2006**, *45*, 2897–2901.
(54) Nashner, M. S.; Frenkel, A. I.; Adler, D. L.; Shapley, J. R.; Nuzzo, R. G. *J. Am. Chem. Soc.* **1997**, *119*, 7760–7771.
(55) Menning, C. A.; Chen, J. G. G. *J. Chem. Phys.* **2009**, *130*, 174709.
(56) Menning, C. A.; Chen, J. G. *J. Power Sources* **2010**, *195*, 3140–3144.
(57) Korotkikh, O.; Farrauto, R. *Catal. Today* **2000**, *62*, 249–254.
(58) Siani, A.; Alexeev, O. S.; Captain, B.; Lafaye, G.; Marecot, P.; Adams, R. D.; Amiridis, M. D. *J. Catal.* **2008**, *255*, 162–179.
(59) Zhang, H.; Fu, Q.; Cui, Y.; Tan, D. L.; Bao, X. H. *J. Phys. Chem. C* **2009**, *113*, 8296–8301.
(60) Ma, T.; Fu, Q.; Su, H. Y.; Liu, H. Y.; Cui, Y.; Wang, Z.; Mu, R. T.; Li, W. X.; Bao, X. H. *ChemPhysChem* **2009**, *10*, 1013–1016.
(61) Yao, Y. X.; Fu, Q.; Wang, Z.; Tan, D. L.; Bao, X. H. *J. Phys. Chem. C* **2010**, *114*, 17069–17079.
(62) Kitchin, J. R.; Khan, N. A.; Barteau, M. A.; Chen, J. G.; Yakshinksiy, B.; Madey, T. E. *Surf. Sci.* **2003**, *544*, 295–308.
(63) Ma, T.; Fu, Q.; Cui, Y.; Zhang, Z.; Wang, Z.; Tan, D. L.; Bao, X. H. *Chin. J. Catal.* **2010**, *31*, 24–32.
(64) Bender, M.; Alshamery, K.; Freund, H. J. *Langmuir* **1994**, *10*, 3081–3085.
(65) Wruck, D. A.; Rubin, M. *J. Electrochem. Soc.* **1993**, *140*, 1097–1104.
(66) Hagendorf, C.; Shantyr, R.; Neddermeyer, H.; Widdra, W. *Phys. Chem. Chem. Phys.* **2006**, *8*, 1575–1583.
(67) Agnoli, S.; Sambi, M.; Granozzi, G.; Schoiswohl, J.; Surnev, S.; Netzer, F. P.; Ferrero, M.; Ferrari, A. M.; Pisano, C. *J. Phys. Chem. B* **2005**, *109*, 17197–17204.
(68) Fu, Q.; Wagner, T. *Surf. Sci. Rep.* **2007**, *62*, 431–498.
(69) Rodriguez, J. A.; Ma, S.; Liu, P.; Hrbek, J.; Evans, J.; Perez, M. *Science* **2007**, *318*, 1757–1760.
(70) Netzer, F. P. *Surf. Rev. Lett.* **2002**, *9*, 1553–1563.
(71) Tsilimis, G.; Kutzner, J.; Zacharias, H. *Appl. Phys. A—Mater.* **2003**, *76*, 743–749.
(72) Tsilimis, G.; Fecher, G. H.; Braun, J.; Kutzner, J.; Zacharias, H. *Appl. Phys. A—Mater.* **2004**, *78*, 177–181.
(73) Grunes, J.; Zhu, J.; Yang, M. C.; Somorjai, G. A. *Catal. Lett.* **2003**, *86*, 157–161.
(74) Su, H. Y.; Gu, X. K.; Ma, X. F.; Zhao, Y. H.; Bao, X. H.; li, W. X. *Catal. Today* **2011**, DOI: 10.1016/j.cattod.2010.10.069.
(75) Menning, C. A.; Chen, J. G. *J. Chem. Phys.* **2008**, *128*, 164703.
(76) Liu, Z. P.; Hu, P. *J. Chem. Phys.* **2001**, *115*, 4977–4980.
(77) Arishtirova, K.; Pawelec, B.; Nikolov, R. N.; Fierro, L. G.; Damyanova, S. *React. Kinet. Catal. Lett.* **2007**, *91*, 241–248.
(78) Mu, R. T.; Fu, Q.; Liu, H. Y.; Tan, D. L.; Zhai, R. S.; Bao, X. H. *Appl. Surf. Sci.* **2009**, *255*, 7296–7301.
(79) Ma, Y. G.; Balbuena, P. B. *Surf. Sci.* **2008**, *602*, 107–113.
(80) Mani, P.; Srivastava, R.; Strasser, P. *J. Phys. Chem. C* **2008**, *112*, 2770–2778.
(81) Strasser, P. *Rev. Chem. Eng.* **2009**, *25*, 255–295.
(82) Strasser, P.; Koh, S.; Anniyev, T.; Greeley, J.; More, K.; Yu, C. F.; Liu, Z. C.; Kaya, S.; Nordlund, D.; Ogasawara, H.; Toney, M. F.; Nilsson, A. *Nature Chem.* **2010**, *2*, 454–460.
(83) Arenas-Alatorre, J.; Gomez-Cortes, A.; Avalos-Borja, M.; Diaz, G. *J. Phys. Chem. B* **2005**, *109*, 2371–2376.
(84) Somorjai, G. A.; Park, J. Y. *J. Chem. Phys.* **2008**, *128*, 182504.